A Stator Current Vector Orientation Based Multi-objective Integrative Suppressions of Flexible Load Vibration and Torque Ripple for PMSM Considering Electrical Loss

Yang Yu, *Member, IEEE*, Leyao Cong, Xia Tian, Zengqiang Mi, Yang Li, *Senior Member, IEEE*, Zhen Fan, and Hui Fan

***Abstract*—To store energy from the grid into spiral torsion spring (STS) smoothly and efficiently via PMSM, a multi-objective control problem of flexible load's vibration, PMSM's torque ripple, and electrical loss is raised, where the current studies on vibration and torque ripple are mostly addressed separately, not to mention electrical loss. This research attempts to propose a multi-objective integrative control scenario that can simultaneously solve these problems satisfactorily in a unitary nonlinear control framework. Firstly, a dynamic mathematical model of PMSM is built under stator current vector orientation, and then the model of PMSM is combined with the vibration model of STS to establish the overall system model of STS driven by PMSM with considering motor's electrical loss. Then, a backstepping control principle-based multi-objective integrative control approach is proposed to realize the suppression of flexible load's vibration and the reduction of PMSM's torque ripple and electrical loss concurrently. Meanwhile, this research also designs a wide range speed identification method based on the least square algorithm with a forgetting factor. Simulation and experimental results have verified that the proposed integrative control method enables the state variables to track their respective references quickly and accurately, both torque ripple and load vibration are effectively suppressed, and the operating efficiency of the whole system is improved.**

***Index Terms*—PMSM, Vibration, Torque ripple, Electrical loss, Backstepping control.**

Manuscript was submitted for review on 01, January, 2020.

This work was supported in part by the Natural Science Foundation of Hebei Province in China under Grant E2019502163, in part by "Double-First Class" Scientific Research Project in School of Electrical and Electronic Engineering of North China Electric Power University under Grant 180718 and in part by the Headquarter of Science and Technology Project for Sate Grid Corporation of China under Grant KJGW 2018-014.

Yang Yu is with an Associate Professor in North China Electric Power University(e-mail: yym0401@163.com)

Leyao Cong and Xia Tian are with graduate student in North China Electric Power University(e-mail: 738581833@qq.com, 1319549621@qq.com)

Zengqiang Mi is with a professor and doctoral tutor in North China Electric Power University(e-mail: mizengqiang@sina.com)

Yang Li is with an Associate professor at the School of Electrical Engineering, Northeast Electric Power University(e-mail: liyang@neepu.edu.cn)

Zhen Fan is pursuing the doctor degree in Lehigh University(e-mail: zhf217@lehigh.edu)

Digital Object Identifier 10.30941/CESTEMS.2020.00021

I. Introduction

FOR a modern power system, the distinguishing characteristics of intermittence and uncontrollability for new renewable energies [1] will threat the power balance between the generating side and the load side. This problem could be tackled by the energy storage technologies [2], [3]. Spiral torsion spring (STS) is known for its features of large storage capacity, high power density, and long lifetime. Nowadays, STS used for electrical energy storage has been widely investigated [4]-[7] and recognized.

The application of STS to store electrical energy is plotted in Fig. 1, where permanent magnet synchronous motor (PMSM) is used as the driving motor, due to its advantages of simple structure, large ratio of torque to inertia and low loss [8]. Electrical energy from the grid is stored into STS with the form of elastic potential energy, and PMSM should be controlled reasonably to wind up STS. For achieving energy storage stably and efficiently, three control problems are required to be solved. It can be seen that main control targets in the context are all on the motor side, so the control method proposed in this research is for the inverter.

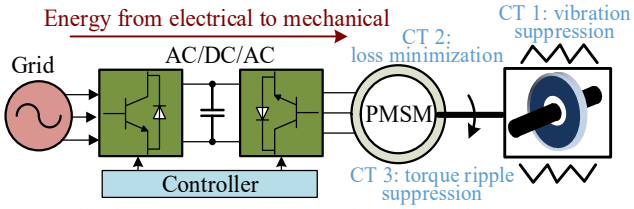

Fig. 1. Multi-objective control of STS used for electrical energy storage, CT: Control Target.

The first problem is the suppression of STS's vibration that stems from the inherent flexibility of STS. Due to the section-size of STS far smaller than its length, when the spring is subjected to the external force and wound up into the spindle, the intrinsic mechanical vibration with certain amplitude and low-frequency will be induced. Hence, it is necessary to construct a mathematical model embodying the vibration mode and design a corresponding controller to suppress the vibration. The previous studies have shown [9] that STS can normally be equivalent to a slender beam and there are two ways to describe its modal vibration. One way is to use the Lagrange equation to build a dynamical equation. Another one is usually realized by

finite element software like ANSYS. But it is difficult to combine the vibration mode obtained by the above methods with the motor to establish a mathematical model for the electromechanical system and it is more unlikely to suppress load vibration.

The second problem is the inhibition of torque ripple in PMSM. The present studies mainly focus on two categories: optimizing the structure of motor [10], [11] and improving the control approach in the expression of electromagnetic torque [12]-[16]. The second category of methods is more suitable for the motor in use. An optimized harmonic current for torque ripple suppression is derived in [12] by using the speed harmonics. Torque ripple caused only by the harmonics is considered, but many other factors have not been mentioned. A control method combining PI control with iterative learning control is proposed in [13], but PI control has relatively weak adaptability to disturbances, and many parameters need to be set. Some other methods have been investigated in [14]-[16], and there are also some defects such as an existing error in compensation, inaccurate detection of zero-crossing of current.

The third problem is the reduction of operating loss in PMSM. The loss of a motor consists of the electrical loss and the mechanical loss. The mechanical loss is not easy to calculate quantitatively and its proportion to the total loss is relatively small. The key to the loss control is to decrease the electrical loss including the iron loss and copper loss if ignoring the damping windings. Maximum Torque Per Ampere technique [17] (MTPA) and Maximum Torque Per Voltage technique [18] (MTPV) are two practical control strategies. But these two techniques are only able to minimize the copper loss and iron loss respectively. Online searching-based minimum power control [19], [20] is used as a typical control strategy to minimum the electrical loss, but this control method has a long-running time and needs to detect the input power. In particular, it's not suitable for frequently dynamic changing situations. The search method was demoted to the background in recent years with the popularization of the loss model-based control [21]-[22]. By establishing a loss model, this control method has wider adaptability and faster response speed. In [21], the loss minimization problem is programmed as a convex nonlinear optimization problem; the iron loss resistance is obtained in [22] by using the Artificial Neural Networks (ANNs); then an optimal current is acquired by using Lagrange optimization. However, these two algorithms are a little redundant.

Currently, the vibration and torque ripple mentioned above are dealt with independently. In Section V, the simulations have proved that these two problems are actually interacting with each other and should be comprehensively investigated. Otherwise, with regard to anyone of those problems, the overall control performance might be weakened. Furthermore, the current studies on these two problems mostly ignore the electrical loss of PMSM, which is uneconomical. The simulations also show that the electrical loss of PMSM accounts for a non-negligible proportion of the total loss, and it can also adversely affect the control accuracy. Therefore, it is necessary to establish a unified control method to address the vibration and torque ripple simultaneously with consideration of the electrical loss.

Aiming directly at regulating the stator current, *I/f* control is a recently proposed control method used for smooth and sensor-less startup [23]. This control method is insensitive to motor parameters and rotor speed, and its arithmetic is relatively simple. In essence, the conventional *I/f* control is a type of open-loop control, which means the amplitude and frequency of the current in *I/f* control cannot be regulated automatically and the speed of the rotor is liable to be disturbed. Hence, *I/f* control is an appropriate framework in this research but still needs some improvements. Besides all these factors, a wide-range speed identification method based on the least square algorithm with a forgetting factor is devised to enhance the stability of conventional *I/f* control, which forms an improved control framework called the closed-loop control. And the proposed algorithm will be introduced specifically in Section IV.

The contribution of the study is to propose a multi-objective nonlinear integrative control scenario based on a closed-loop *I/f* control framework of PMSM. Specifically, the novel is reflected in threefold: (1) An overall mathematical model of STS driven by PMSM directly is firstly established with integrative consideration of STS vibration, PMSM's electrical loss, and torque ripple. (2) A closed-loop *I/f* control framework of PMSM is presented, and on the basis of the control framework, a multi-objective backstepping principle-based integrative controller (called as 'integrative controller') is proposed to reduce the electrical loss of PMSM and suppress vibration of flexible load and torque ripple of PMSM simultaneously. (3) A wide-range speed identification method based on the least square algorithm with a forgetting factor under this framework is devised. The feasibility of the proposed algorithm is validated by simulations and hardware experiments. The proposed control method ensures stable and secure energy storage. Both steady-state and dynamic performance are improved, and the operating efficiency of PMSM is enhanced.

The arrangement of the paper is as below: an overall mathematical model of the system is described in Section II. The integrative control scheme that considers the electrical loss of PMSM to drive flexible STS and suppresses vibration of flexible load and torque ripple of PMSM is proposed in Section III. The speed identification method is demonstrated in Section IV. The simulation and experimental analysis are conducted in Section V. The last section sums up the research results.

II. Modeling Of The Whole System

For the overall energy storage system shown in Fig. 1, PMSM and STS are connected by its spindle directly shown in Fig. 2, which means that either the torque ripple of PMSM or the vibration of STS will act on the spindle and interact with each other. Therefore, their direct connection form requires a reasonable overall model to integrate the existing STS model with PMSM's model.

A. Vibration Model of STS

The previous research has shown that STS will appear an

inherent vibration with low frequency and large amplitude under the action of external force. Furthermore, this inherent vibration will cause negative impact on the system. Therefore, acquiring the vibration frequency and suppressing the inherent vibration are the key points of this research.

In Fig. 2, the spindle of PMSM connects with STS at its endpoint o, and o' indicates the center on the cross-section of point o. A stationary coordinate system $x'o'y'$ and a dynamic coordinate system xoy rotating synchronously with the rotor are both built. θ_r indicates the rotating angle. When STS is wound up by the output torque T_L of PMSM, $s(x, t)$ is used to express the displacement changed in xoy, and it also shows the deflection at x.

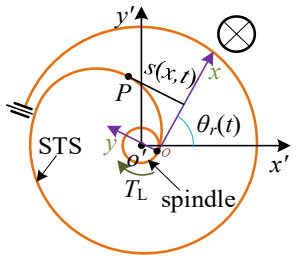

Fig. 2. Diagram of direct connection of spring with PMSM.

It is supposed that STS is formed by bending a slender beam into a spiral shape. When the system works in a wide range, the transverse vibration is much more obvious than the longitudinal vibration. Therefore, for STS: (1) Only the transverse vibration of the spring is considered, and the longitudinal vibration is ignored; (2) The transverse vibration is a small deformation; (3) The length of the spring is far greater than its cross-section size. Therefore, the spring can be regarded as an Euler-Bernoulli beam and its vibration equation is written as below [24]:

$$\frac{\partial^2}{\partial x^2}\left(EI\frac{\partial^2 s(x,t)}{\partial x^2}\right)+\rho S_p\frac{\partial^2 s(x,t)}{\partial t^2}=f(x,t) \tag{1}$$

where E, I and ρ are the elasticity modulus, cross-sectional moment of inertia and density of spring material respectively; $I=bh^3/6$, where b and h indicate the width and thickness of the strip S_p is the sectional area in per unit length, $f(x,t)$ is the external force distributed in STS.

The boundary conditions of STS can be described as:

$$\begin{cases} s(0,t)=0, s(L,t)=0 \\ \dfrac{\partial s(0,t)}{\partial x}=0, \dfrac{\partial s(L,t)}{\partial x}=0 \end{cases} \tag{2}$$

where L indicates the length of STS.

According to the vibration theory, $s(x,t)$ is expressed as:

$$s(x,t)=\sum_{i=1}^{\infty}\phi_i(x)\eta_i(t)=\left[\boldsymbol{\phi}(x)\right]^{\mathrm{T}}\boldsymbol{\eta}(t) \tag{3}$$

where $\boldsymbol{\phi}(x)$ and $\boldsymbol{\eta}(t)$ are the modal function and modal coordinate individually.

In accordance with [25], $f(x,t)$ can be regarded. Substituting (3) into (1), the relation of $\boldsymbol{\phi}(x)$ to $\boldsymbol{\eta}(t)$ will be obtained through variable separation:

$$\ddot{\boldsymbol{\eta}}(t)/\boldsymbol{\eta}(t)=-\left(EI\ddot{\boldsymbol{\phi}}(x)\right)''/\rho S_p\boldsymbol{\phi}(x) \tag{4}$$

where $\dot{(\ )}$ indicates $d(\ )/dt$ in the context. For (4), its left side is only related to the time t and its right side is only related to x. It means that the solution of (4) is a constant, which can be supposed as $-a^2$. Then, (4) can be rewritten and its eigenvalue equation is as follows:

$$\begin{cases} \left(\ddot{\boldsymbol{\phi}}(x)\right)''-a^2\rho\dfrac{S_p\boldsymbol{\phi}(x)}{EI}=\ddddot{\boldsymbol{\phi}}(x)-\chi^4\boldsymbol{\phi}(x)=0 \\ \ddot{\boldsymbol{\eta}}(t)+a^2\boldsymbol{\eta}(t)=0,\ \gamma^4-\chi^4=0 \end{cases} \tag{5}$$

In accordance with (2), (5), $\boldsymbol{\phi}(x)$ and $\boldsymbol{\eta}(t)$ can be solved:

$$\begin{cases} \boldsymbol{\phi}(x)=a_1\sin(\gamma x)+a_2\cos(\gamma x) \\ \qquad +a_3\sinh(\gamma x)+a_4\cosh(\gamma x) \\ \boldsymbol{\eta}(t)=a_5\sin(\omega t)+a_6\cos(\omega t)=a_7\sin(\omega t+\varphi) \\ a_1=-a_3, a_2=-a_4, \cos(\gamma l)\cosh(\gamma l)=1 \end{cases} \tag{6}$$

According to (5), the angular velocity ω and the N-th order mode could be written as:

$$\omega=\gamma^2\sqrt{\frac{EI}{\rho S_p}} \tag{7}$$

For any point P on STS shown in Fig. 2, its coordinates (X_P, Y_P) in the frame xoy is:

$$\begin{cases} X_P=x\cos\theta_r-s(x,t)\sin\theta_r \\ Y_P=x\sin\theta_r+s(x,t)\cos\theta_r \end{cases} \tag{8}$$

In accordance with (8), when wounding up STS, the kinetic energy T exerted by PMSM and potential energy V stored in the spring can be written as:

$$\begin{cases} T=\dfrac{1}{2}\displaystyle\int_0^l\rho bh\left(x^2\dot{\theta}_r^2+\dot{s}^2+2\dot{s}x\dot{\theta}_r+s^2\dot{\theta}_r^2\right)dx \\ V=\dfrac{1}{2}\displaystyle\int_0^l EI\left(\frac{\partial^2 s}{\partial x^2}\right)^2dx \end{cases} \tag{9}$$

Lagrange equation can be displayed as below:

$$\frac{d}{dt}\left(\frac{\partial(T-V)}{\partial\dot{q}_i}\right)-\frac{\partial(T-V)}{\partial q_i}=Q_i,(i=1,2,\cdots,N+1) \tag{10}$$

where q_1 is θ_r, q_i $(2\le i\le N+1)$ is the (i-1)-th order modal coordinate η_{i-1}, Q_i is the equivalent external force.

For s is small, items containing s can be ignored. According to (10), for q_1 and q_i, the following equations can be obtained:

$$\begin{cases} \dfrac{T_e-T_{sp}}{\rho bh}=\left[\begin{array}{l}\displaystyle\sum_{i=1}^{N}\left(\ddot{\eta}_i\int_0^l x\phi_i dx+\int_0^l 2s\dot{\theta}_r\phi_i\dot{\eta}_i dx\right) \\ +\ddot{\theta}_r\displaystyle\int_0^l x^2dx\end{array}\right] \\ B_i\displaystyle\sum_{i=1}^{N}\ddot{\eta}_i+A_i\ddot{\theta}_r+D_i\eta_i-E_i\sum_{i=1}^{N}\eta_i(t)\dot{\theta}_r^2=0 \end{cases} \tag{11}$$

where T_{sp} is the bending torque of STS, $T_{sp}=k_{sp}\cdot\theta_r$, k_{sp} is a constant representing the elasticity of STS. With the energy stored into the spring, its torque T_{sp} will become larger. $\rho bh\int_0^l x^2dx=M$, $\rho bh\int_0^l x\phi_i dx=A_i$, $\rho bh\int_0^l\phi_i^2dx=B_i$,

$EI\int_0^l \ddot{\phi}_i^2 dx = D_i$, $\rho bh\int_0^l \phi_i dx = E_i$.

B. Implementation Condition under Minimum Loss Operation for PMSM

When PMSM drives STS to store energy, the output torque is time-varying. The overall operating condition is much more complicated than the constant output torque. According to Section I, online searching-based minimum power control is inappropriate. Therefore, based on the idea of the loss model-based control, this research intends to derive a brief optimal stator current expression integrating with the loss model to realize the real-time electrical loss control.

Fig. 3 shows the equivalent circuits of PMSM in *dq* axes including iron loss resistance. The equations of PMSM considering the iron and copper losses can be obtained as below.

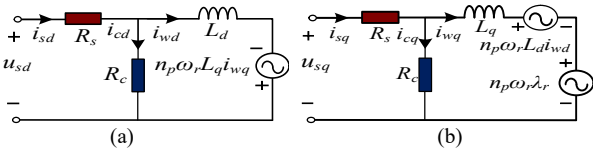

Fig. 3. Equivalent circuits of PMSM in dq axes. (a) d-axis equivalent circuit, (b) q-axis equivalent circuit.

$$\left\{R_c i_{cd} = -n_p\omega_r L_q i_{wq} \ , R_c i_{cq} = n_p\omega_r\left(\lambda_r + L_d i_{wd}\right)\right\} \quad (12)$$

where i_{wd} and i_{wq} are the active currents in d and q axes, i_{cd} and i_{cq} are the iron loss currents in d and q axes, L_d and L_q are the inductor components in d and q axes, R_c is the equivalent iron loss resistance, n_p is the number of pole pairs, λ_r is the linkage of permanent magnet, ω_r is the mechanical angular velocity of the rotor

The effective electromagnetic torque T_e can be described as:

$$T_e = 3n_p\lambda_r i_{wq}/2 \quad (13)$$

The copper loss P_{Cu}, the iron loss P_{Fe} and the total electrical loss P_{Loss} of PMSM can be calculated as follows:

$$\begin{cases} P_{Loss} = P_{Cu} + P_{Fe} \ , P_{Fe} = 3R_c\left(i_{cd}^2 + i_{cq}^2\right)/2 \\ P_{Cu} = 3R_s\left[\left(i_{cd} + i_{wd}\right)^2 + \left(i_{cq} + i_{wq}\right)^2\right]/2 \end{cases} \quad (14)$$

i_{wq} can be calculated through T_e shown in (13). By a partial derivative of P_{Loss} with respect to i_{wd}, the optimal stator current under the condition of minimum total electrical loss is:

$$i_{wdref} = -\frac{n_p^2\omega_r^2 L_d\left(R_s + R_c\right)\lambda_r}{R_s R_c^2 + n_p^2\omega_r^2 L_d^2\left(R_s + R_c\right)} \quad (15)$$

where R_s is the stator resistance. Hence,

$$i_{dref} = i_{wdref} + i_{cd} \quad (16)$$

C. Stator Current Vector Orientation Based Dynamical Modeling of PMSM

dqo is the original rotating frame of PMSM. To investigate the stator current vector $\boldsymbol{i}_s$, a new rotating coordinate frame d^*q^*o is introduced in the section, which is drawn in Fig. 4. d^* and q^* axes are the new real and imaginary axes. The angle between q^* axis and d axis is described as θ_L.

In d^*q^*o, the relation of voltage to current in stator winding is presented in [26]. Due to the stator current i_s is oriented along q^* axis, it indicates that the stator current i_{sq^*} in q^* axis equals to i_s and the stator current i_{sd^*} in d^* axes is zero. According to Fig. 4, stator voltages can be rewritten as:

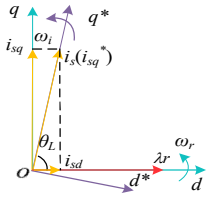

Fig. 4. New introduced coordinate frame d^*q^*o based on original coordinate frame *dqo*.

$$u_{sd^*} = -L_{q^*} i_s\dot{\theta}_L - n_p\lambda_r\omega_r\cos\theta_L - n_p\omega_r L_{q^*} i_s \quad (17)$$

$$u_{sq^*} = R_s i_s + L_{q^*}\dot{i}_s + n_p\lambda_r\omega_r\sin\theta_L \quad (18)$$

where u_{sd^*}, u_{sq^*} are the stator voltages in d^* and q^* axes individually, ω_i is the rotating speed in d^*q^*o frame. L_{d^*} is the inductor in d^*axis, L_{q^*} is the inductor in q^* axis.

Besides, the relationship among θ_L, ω_r, and ω_i is written as:

$$\dot{\theta}_L = n_p\left(\omega_i - \omega_r\right) \quad (19)$$

Equations from (17) to (19) construct the dynamical model of PMSM in the new framework. To keep the stability of PMSM at running, the conventional *I/f* control scheme requires a proper command to accelerate the speed and should restrict θ_L in $(0°,180°)$.

D. Overall Mathematical Model of STS Driven by PMSM Considering STS's Vibration

In general, the vibration weakens the operating performance of the system. Especially for the first-order vibration mode, it impacts much more than other higher-order modes on the control performance [27]. Hence, the study only considers the first-order mode, and (11) can be simplified and rewritten as:

$$\begin{cases} \ddot{\theta}_r M + A_1\ddot{\eta}_1 = T_e - T_{sp} \\ B_1\ddot{\eta}_1 + A_1\ddot{\theta}_r + D_1\eta_1 - E_1\eta_1\dot{\theta}_r^2 = 0 \end{cases} \quad (20)$$

Then the whole dynamical model of the system can be derived by the association of (17), (18), (19) with (20).

III. Integrative Control Of Vibration And Torque Ripple With Minimum Electrical Loss

A. Backstepping principle Based Vibration Controller with Minimum Electrical Loss

Based on the whole mathematical model and backstepping principle, a vibration controller with minimum electrical loss is proposed. e_θ, e_ω, and e_i indicate the tracking errors of angle θ_L, speed ω_r, and i_{s0}, where i_{s0} is the amplitude of the fundamental current. θ_L^*, ω_r^* and i_{s0}^* are the anticipated references. k_θ, k_ω and k_i are pending positive numbers.

The first virtual control variable θ_L^* is designed to stabilize the speed and realize the minimum loss, which is shown as:

$$\theta_L^* = \arccos\left(i_{dref}/i_{s0}^*\right) \quad (21)$$

Due to $e_\theta = \theta_L - \theta_L^*$, the derivative of e_θ can be written as:

$$\dot{e}_\theta = \dot{\theta}_L - \dot{\theta}_L^* = n_p\left(\omega_i - \omega_r\right) - \dot{\theta}_L^* \quad (22)$$

Then, the second virtual control variable ω_r^* is obtained:

$$\omega_r^* = \left(n_p\omega_i - \dot{\theta}_L^* + k_\theta e_\theta\right)/n_p \tag{23}$$

By substituting (23) into (22), we can get:

$$\dot{e}_\theta = -k_\theta e_\theta \tag{24}$$

According to Fig. 4 and (13), T_e is rewritten as:

$$T_e = 3n_p\lambda_r\left(i_{s0}\sin\theta_L - i_{cq}\right)/2 \tag{25}$$

Because of $e_\omega = \omega_r - \omega_r^*$, the derivative of e_ω is written as:

$$\dot{e}_\omega = \frac{B_1T_e - B_1T_{sp} + A_1D_1x_1}{MB_1 - A_1^2} - \dot{\omega}_r^* \tag{26}$$

where $x_1 = \eta_1$. Then, the third virtual control variable i_{s0}^* can be acquired:

$$i_{s0}^* = \frac{2\begin{pmatrix}\left(MB_1 - A_1^2\right)\left(\dot{\omega}_r^* - k_\omega e_\omega\right)\\ -A_1D_1x_1 + T_{sp}B_1\end{pmatrix} + 3n_p\lambda_r i_{cq}B_1}{3n_p\lambda_r B_1\sin\theta_L} \tag{27}$$

Equation (27) indicates that i_{s0} will increase with the bending torque T_{sp}. According to (14), P_{Loss} is not a constant, it will also change with i_{s0}.

In terms of (16) and (27), (21) can be rewritten more specifically. By substituting (27) into (26), we can get:

$$\dot{e}_\omega = -k_\omega e_\omega \tag{28}$$

Due to $e_i = i_{s0} - i_{s0}^*$, the derivative of e_i is written as:

$$\dot{e}_i = \dot{i}_{s0} - \dot{i}_{s0}^* = \frac{u_{sq^*0} - R_s i_{s0} - n_p\lambda_r\omega_r\sin\theta_L}{L_{q^*}} - \dot{i}_{s0}^* \tag{29}$$

Ultimately, the control variable u_{sq0*} can be selected as:

$$u_{sq^*0} = -L_{q^*}k_i e_i + L_{q^*}\dot{i}_{s0}^* + R_s i_{s0} + n_p\lambda_r\omega_r\sin\theta_L \tag{30}$$

By substituting (30) into (29), we can obtain:

$$\dot{e}_i = -k_i e_i \tag{31}$$

B. Backstepping Principle-Based Torque Ripple Suppression Controller

From the viewpoint of magnetic co-energy and considering $L_d = L_q$ in surface-mounted PMSM, T_e of PMSM is described as [28]:

$$T_e = K_p\left\{\left(\psi_d + p\psi_q\right)i_s\sin\theta_L + \left(p\psi_d - \psi_q\right)i_s\cos\theta_L\right\} + T_{cog} \tag{32}$$

where $p(\,)$ indicates $d(\,)/d\theta$ in the context, K_p=3n_p/2, ψ_d and ψ_q indicate the flux linkages of d and q axes respectively, T_{cog} indicates the cogging torque. Due to,

$$\begin{cases} i_s = i_{s0} + \sum_k I_{sk}\cos\left(k\theta - \phi_{sk}\right), T_{cog} = \sum_k T_{ck}\cos\left(k\theta - \phi_{ck}\right) \\ \psi_d = \psi_0 + \sum_k \psi_{dk}\cos\left(k\theta - \phi_{\psi k}\right), \psi_q = \sum_k \psi_{qk}\sin\left(k\theta - \phi_{\psi k}\right) \end{cases} \tag{33}$$

where k is the harmonic order, I_{sk} and ϕ_{sk} are the k-th harmonic current and its phase angle, ψ_0 is the average magnetic linkage in d axis, ψ_{dk} and ψ_{qk} are the k-th harmonic components of permanent magnet flux in d and q axes, $\phi_{\psi k}$ is the k-th flux harmonic's phase angle, T_{ck} and ϕ_{ck} are the k-th harmonic's magnitude and phase angle in cogging torque.

By substituting (33) into (32), a more specific expression of T_e will be obtained. In practice, ψ_{dk}, ψ_{qk}, and I_{sk} account for small proportions in their total values. Two or three product terms among ψ_{dk}, ψ_{qk} and I_{sk} will be smaller and can be disregarded, then, the arranged expression of T_e is shown as:

$$T_e = T_0 + \sum_k\left(\sqrt{D_k^2}\cos\left(k\theta - \phi_k\right) + \sqrt{E_k^2 + F_k^2}\cos\left(k\theta - \varphi_k\right)\right) \tag{34}$$

where T_0 is the active component in electromagnetic torque, ϕ_k and φ_k are two angles, and

$$\begin{cases} D_k = K_p I_{sk}\psi_0\sin\theta_L, \tan\varphi_k = F_k/E_k, \tan\phi_k = \tan\phi_{sk} \\ E_k = K_p i_{s0}\begin{pmatrix}\sin\theta_L\left(\psi_{dk} + k\psi_{qk}\right)\cos\phi_{\psi k}\\ -\cos\theta_L\psi_{qk}\cos\phi_{\psi k}\end{pmatrix} \\ \quad - K_p i_{s0}\cos\theta_L k\psi_{dk}\sin\phi_{\lambda k} + T_{ck}\cos\phi_{ck} \\ F_k = K_p i_{s0}\begin{pmatrix}\sin\theta_L\left(\psi_{dk} + k\psi_{qk}\right)\sin\phi_{\psi k}\\ +\cos\theta_L\psi_{qk}\sin\phi_{\psi k}\end{pmatrix} \\ \quad + K_p i_{s0}\cos\theta_L k\psi_{dk}\cos\phi_{\psi k} + T_{ck}\sin\phi_{ck} \end{cases} \tag{35}$$

The optimal angle ϕ_{sk}^{opt} of the k-th harmonic current could be obtained in terms of (35). One of the control objectives is to remove all the harmonics in T_e, so D_k is no less than zero since θ_L is restricted in $(0°,180°)$. Then the k-th harmonic in (34) should satisfy:

$$\left\{D_k = \sqrt{E_k^2 + F_k^2}\ ,\ \phi_k - \varphi_k = \pi\right\} \tag{36}$$

Solving (36) through building an auxiliary function with introducing a Lagrange multiplier γ, the optimal harmonic current I_{sk} can be gained and described as:

$$I_{sk}^{opt} = \sqrt{E_k^2 + F_k^2}\Big/\left(K_p\psi_0\sin\theta_L\right) \tag{37}$$

The research have shown that only certain harmonics occupy the dominant position in dqo frame for PMSM, such as the 6th, 12th and 18th [29]. Based on the constraint condition derived in (37), a torque ripple suppression controller based on backstepping principle will then be proposed. $i_{sk}^* = I_{sk}^{opt}$ is the anticipated reference of i_{sk}. θ_{Lk}^* is the anticipated reference of θ_{Lk}, where θ_{Lk} is the angle between d axis and harmonic current and $\theta_{Lk}^* = k\theta_L^*$. e_{ik} and $e_{\theta k}$ are the tracking error variables respectively. k_{ik} and $k_{\theta k}$ are the pending positive control gains.

Due to:

$$\theta_{Lk}^* = k\theta_L^* \tag{38}$$

And $e_{\theta k} = \theta_{Lk} - \theta_{Lk}^*$, the derivative of $e_{\theta k}$ could be expressed as:

$$\dot{e}_{\theta k} = \frac{-u_{sd^*k} - kn_p\lambda_{rk}\omega_r\cos\theta_{Lk} - kn_p\omega_i L_{q^*}i_{sk}}{L_{q^*}i_{sk}} - \dot{\theta}_{Lk}^* \tag{39}$$

The control variable u_{sdk*} can be chosen as:

$$\begin{aligned} u_{sdk^*} = &-L_{q^*}i_{sk}\dot{\theta}_{Lk}^* - kn_p\lambda_{rk}\omega_r\cos\theta_{Lk} - kn_p\omega_i L_{q^*}i_{sk} \\ &+L_{q^*}i_{sk}k_{\theta k}e_{\theta k} \end{aligned} \tag{40}$$

By substituting (40) into (39), (39) will be rewritten as:

$$\dot{e}_{\theta k} = -k_{\theta k}e_{\theta k} \tag{41}$$

Then, the derivative of e_{ik} can be calculated as :

$$\dot{e}_{ik} = \dot{i}_{sk} - \dot{i}_{sk}^* = \frac{u_{sq^*k} - R_s i_{sk} - kn_p\lambda_{rk}\omega_r\sin\theta_L}{L_{q^*}} - \dot{i}_{sk}^* \tag{42}$$

The control variable u_{sqk*} is determined as:

$$u_{sqk*} = R_s i_{sk} + kn_p \lambda_{rk} \omega_r \sin\theta_L + L_{q*} \dot{i}^*_{sk} - L_{q*} k_{ik} e_{ik} \quad (43)$$

By substituting (43) into (42), we can get:

$$\dot{e}_{ik} = -k_{ik} e_{ik} \quad (44)$$

C. Integrative Controller of Vibration and Torque Ripple Suppression with Minimum Loss

On the basis of guaranteeing the minimum electrical loss of PMSM designed on Section III, a multi-objective backstepping principle-based integrative controller is proposed to realize the contemporaneous suppression of STS's vibration and PMSM's torque ripple. The schematic of the control scenario is plotted in Fig. 5, where the speed identification algorithm will be discussed in the next section.

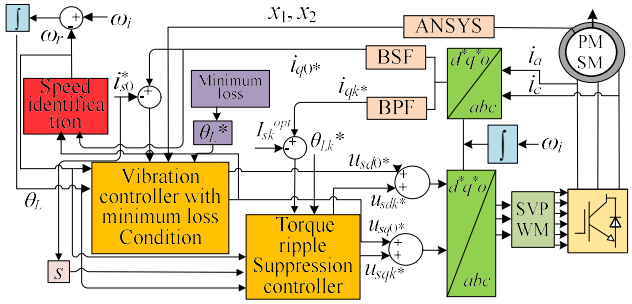

Fig. 5. Structural diagram of the integrative controller under closed-loop I/f control framework, BSF: band-stop filter, BPF: band-pass filter.

(a) Structural diagram of the proposed controller, **(b)** Mathematical model of controller with minimum losses conditions, **(c)** Mathematical model of torque ripple suppression controller

In terms of (30) and (39), eventual voltage control equation of the integrative controller is written as:

$$u_{sq*} = -L_{q*} k_i e_i + L_{q*} \dot{i}^*_{s0} + R_s i_{s0} + n_p \lambda_r \omega_r \sin\theta_L + \sum_k \left(R_s i_{sk} + kn_p \lambda_{rk} \omega_r \sin\theta_L + L_{q*} \dot{i}^*_{sk} - L_{q*} k_{ik} e_{ik} \right) \quad (45)$$

$$u_{sd*} = -L_{q*} i_{s0} \dot{\theta}_L^* - n_p \lambda_r \omega_r \cos\theta_L - n_p \omega_r L_{q*} i_{s0} + \sum_k \begin{pmatrix} -L_{q*} i_{sk} \dot{\theta}_{Lk}^* - kn_p \lambda_{rk} \omega_r \cos\theta_{Lk} - kn_p \omega_i L_{q*} i_{sk} \\ + L_{q*} i_{sk} k_{\theta k} e_{\theta k} \end{pmatrix} \quad (46)$$

D. Determination of controller parameters and its robustness analysis

In terms of (24), (28), (31), (41) and (44), the differential equation with respect to e_θ, e_ω, e_i, $e_{\theta k}$ and e_{ik} can be derived as:

$$\begin{bmatrix} \dot{e}_\theta \\ \dot{e}_\omega \\ \dot{e}_i \\ \dot{e}_{\theta k} \\ \dot{e}_{ik} \end{bmatrix} = \begin{bmatrix} -k_\theta & 0 & 0 & 0 & 0 \\ 0 & -k_\omega & 0 & 0 & 0 \\ 0 & 0 & -k_i & 0 & 0 \\ 0 & 0 & 0 & -k_{\theta k} & 0 \\ 0 & 0 & 0 & 0 & -k_{ik} \end{bmatrix} \begin{bmatrix} e_\theta \\ e_\omega \\ e_i \\ e_{\theta k} \\ e_{ik} \end{bmatrix} = \boldsymbol{A} \begin{bmatrix} e_\theta \\ e_\omega \\ e_i \\ e_{\theta k} \\ e_{ik} \end{bmatrix} \quad (47)$$

where $\boldsymbol{A}$ is a matrix describing the tracking performance. λ is the eigenvalue of the matrix $\boldsymbol{A}$, and its characteristic equation can be written as:

$$(\lambda + k_\theta)(\lambda + k_\omega)(\lambda + k_i)(\lambda + k_{\theta k})(\lambda + k_{ik}) = 0 \quad (48)$$

To ensure all the eigenvalues of $\boldsymbol{A}$ are located on the left-half plane, we have to choose that k_θ>0, k_ω>0, k_i>0, $k_{\theta k}$>0, and k_{ik}>0. In order to enlarge the stability region, the eigenvalues should keep a certain distance away from the imaginary axis. Therefore, a set of control parameters are determined by the trial and error method and displayed as k_θ = 185, k_ω = 50, k_i = 320, $k_{\theta k}$ = 270, k_{i6} = 440. With these control parameters, the robustness of the integrative controller with the dynamic responses of speed tracking is conducted and demonstrated in Fig. 6, where the parameters variation of PMSM is ±80% of their rated values respectively. It turns out that all tracking errors are able to converge to zero in a very short time, which means that the proposed controller is robust enough for the parameter disturbance variations of PMSM.

IV. Speed Identification Of PMSM Used For The Integrative Controller

Precise speed information is basic to complete the controller

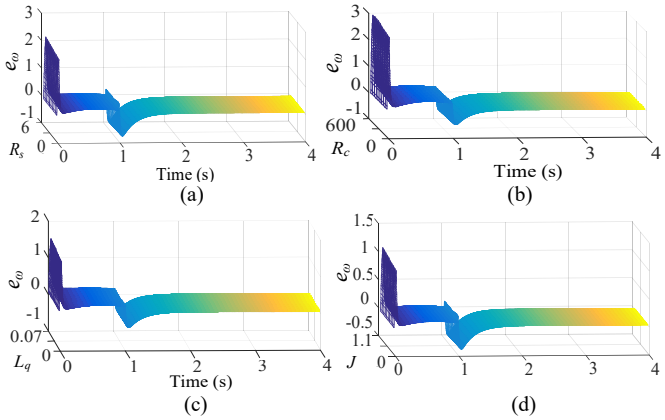

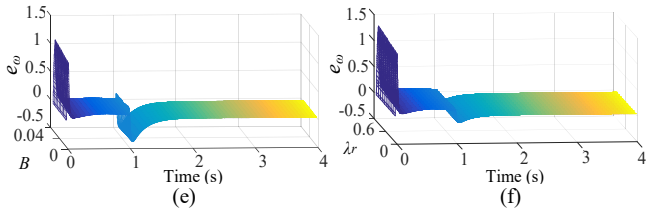

Fig. 6. Speed tracking with parameters variation. (a) R_s, (b) Rc, (c) L_q, (d) J, (e) B, (f) λ_r.

proposed in Section III. For PMSM, current approaches of speed identification are divided into two different types of medium-low speed [30], [31] and medium-high speed [32], [35]. Merely, each proposed method has its defects or limitations. [30], [31] are likely to lead to torque ripple, and increasing speed will weaken the identification effect. The flux linkage in [32], [33] often has an integral error due to the zero drift problem. The algorithms in [34], [35] are too complex and will cause a large calculation amount. The least-squares method with a forgetting factor has been testified to have an outstanding performance in identifying the variables changing with the time. Aiming at the weakness of existing approaches, the least-squares based speed identification method for PMSM under the constructed control framework in the study is designed. First, (17) and (18) are discretized; then based on the identification equations in [36], variables of $\boldsymbol{y}$, $\boldsymbol{\varphi}$ and $\boldsymbol{B}$ for speed identification can be represented as:

$$\begin{cases} \boldsymbol{y}(n)=\begin{bmatrix} u_{sq*}(n)-R_s i_s(n)-L_{q*}\left(i_s(n)-i_s(n-1)\right)/T_s \\ u_{sd*}(n)+n_p\omega_r(n)L_{q*}i_s(n) \\ +L_{q*}i_s(n)\left(\left(\theta_L(n)-\theta_L(n-1)\right)/T_s\right) \end{bmatrix} \\ \boldsymbol{\varphi}(n)=\begin{bmatrix} n_p\lambda_r \\ -n_p\lambda_r \end{bmatrix},\ \hat{\boldsymbol{B}}(n)=\begin{bmatrix} \omega_r(n)\sin\left(\theta_L(n)\right) \\ \omega_r(n)\cos\left(\theta_L(n)\right) \end{bmatrix} \end{cases} \tag{49}$$

where T_s is the sampling time. By substituting (43) into the identification equations in [33], the identification rule of the speed for PMSM is performed.

V. Simulation And Experimental Analysis

A. Modal Analysis Based on ANSYS Software

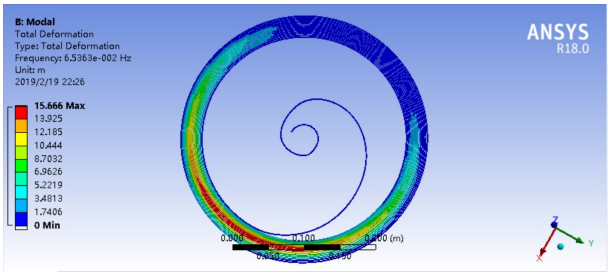

Fig. 7. Simulation result of modal analysis for STS.

ANSYS is a commonly used software for modal analysis, and its Workbench module has been chosen to reveal the vibration mode of STS accurately. The parameters of STS used for energy storage are listed in Table I and the first-order mode analysis is conducted and shown in Fig 7. It shows that the first-order mode frequency of STS is about 0.065 Hz. In accordance with (3) and (7) in Section II, the angular frequency ω of STS is theoretically calculated as 0.387 rad/s, and corresponding first-order vibration frequency is 0.062 Hz. The error of the first-order vibration frequency between the theoretical value and the calculated value is about 6.45%, which proves the correctness of the theoretical result.

TABLE I
PARAMETERS OF STS

Parameters	Value	Parameters	Value
mass density	7850 kg/m^3	length	14.639 m
thickness	0.0018 m	elastic modulus	2×10^{11} N/m^2
width	0.050 m	torque coefficient	3.95

B. Simulation Certification of Control Scheme

To validate the proposed integrative controller, a series of simulations are constructed in MATLAB. The parameters of PMSM are displayed in Table II. R_c is obtained through the linear feature between semi-input power and square of speed emf in the offline method proposed in [37]. The investigation of the study has uncovered that the proportion of the sixth harmonic is the largest in all harmonic components, and it is selected to be suppressed.

TABLE II
PARAMETERS OF PMSM

Parameters	Value	Parameters	Value
inertia	0.51 kg·m^2	permanent magnet	
stator resistance	2.875 Ω	flux linkage	0.3Wb
iron loss resistance	300 Ω	number of pole pairs	50
viscous coefficient	0.02 N/m/s	stator inductance	0.033 H

Three steady-state speed references of 20 r/min, 60 r/min and 150 r/min covering a certain range of speed are chosen to testify the approach of speed identification, and the estimation results are demonstrated in Fig. 8. With the proposed least square algorithm, the speed of PMSM can track its references precisely in a wide range. The proposed algorithm is proved to be practical.

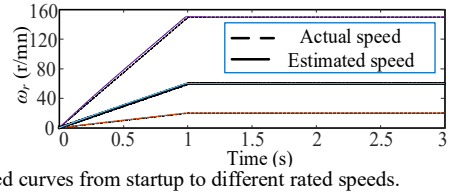

Fig. 8. Speed curves from startup to different rated speeds.

In the second case, Load torque T_L is 15 N·m and PMSM starts up from standstill to 60 r/min to demonstrate the superior control performance of traditional PI-based *I/f* control compared with closed-loop *I/f* control proposed in this research. The comparative results of θ_L, ω_r and i_{s0} are displayed in Fig. 9. Due to the intrinsic open-loop property of traditional *I/f* control, the amplitude of stator current in operation requires larger to avoid the risk of out of step, this will increase energy consumption at the same time. It can be seen that under the open-loop *I/f* control, the current is out of effective control and the operating parameters are oscillating around its actual value. The closed-loop *I/f* control on the other hand used in the study stabilizes the state variables.

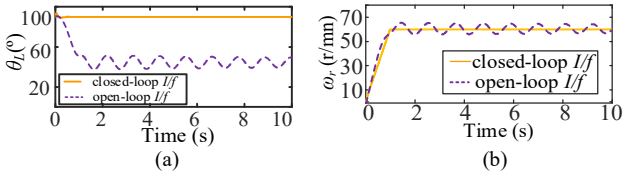

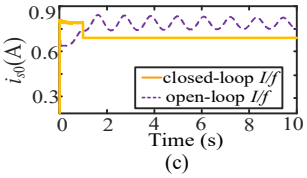

Fig. 9 Comparison between open-loop *I/f* control and closed-loop *I/f* control. (a) θ_L, (b) ω_r, (c) i_{s0}.

The third case only investigates the suppression of vibration of STS. PMSM also starts up from standstill to 60r/min, and the operating parameters regulated with or without the vibration controller are presented in Fig. 10(a)-(d). In this way, PMSM starts up smoothly and operates stably. In order to verify the superiority of the proposed controller, Fig. 10(e) compares the waveform of ω_r under vibration controller and PI controller. It is shown the speed is more stable under the proposed vibration control.

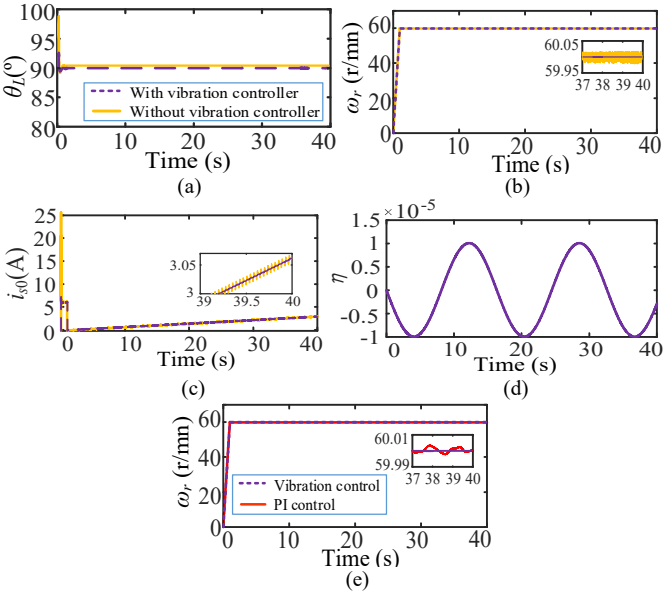

Fig. 10. Waveforms with or without vibration controller in PMSM. (a) θ_L, (b) ω_r, (c) i_{s0}, (d) η, (e) ω_r.

But the operating environment of PMSM is much more complicated in practice. Thus, cogging torque, harmonics, and electrical loss are considered. If only activating the vibration controller, the operating parameters are shown in Figs. 11(a)-(c) again, while the torque ripple δT and total electrical loss P_{Loss} caculted by 14 are plotted in Figs. 11(d)-(e). It turns out that only with the vibration controller, torque ripple and electrical loss still exist in PMSM; furthermore, they will decrease the control accuracy of the vibration controller. Hence, a single vibration controller cannot address the problem of stable operation with multiple disturbances for PMSM.

The fourth case is designed to verify the effectiveness of the minimum loss condition derived in Section II. Load torque T_L is set to 10 N·m and steady-state speed is 60 r/min.

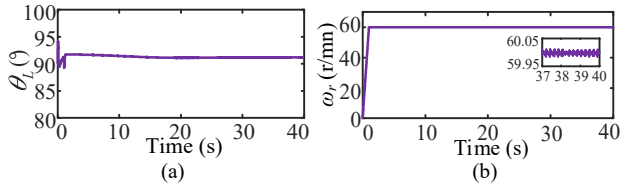

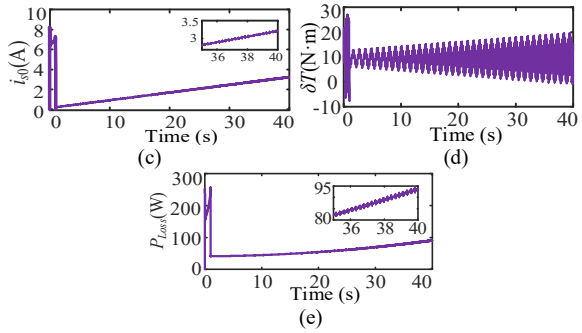

Fig. 11. Waveforms only controlled by vibration controller while considering cogging torque, electrical loss and torque ripple in PMSM. (a) θ_L, (b) ω_r, (c) i_{s0}, (d) δT, (e) P_{Loss}.

Only electrical. loss is taken into account. The control performance with and without minimum loss condition is compared in Fig. 12Electrical loss with minimum loss condition is less than that in traditional backstepping control with no minimum loss. Meanwhile, every operating parameter under minimum loss control converges to its references more stably.

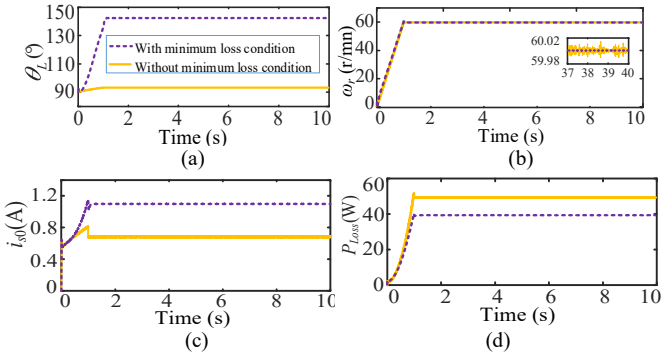

Fig. 12. Comparison with and without minimum loss condition through proposed control. (a) θ_L, (b) ω_r, (c) i_{s0}, (d) P_{Loss}.

In the fifth case, the controller of torque ripple suppression will be tested. Initial load torque T_L is set to be 10 N·m and PMSM starts up from standstill to 60 r/min. At 5 s, T_L decreases to 5 N·m, and T_L recovers to 10 N·m at 15 s. Then, at 25 s, T_L increases to 15 N·m and lasts 10 s. T_L recovers to 10 N·m at 35 s. Fig. 13 shows the results that the operating parameters suffer transient and small oscillations only at the moment of a sudden switch of load torque. In contrast with Fig. 11(d), the proposed controller can suppress the torque ripple effectively. With the aid of the controller, the peak-to-peak value of torque ripple is no more than 0.1 N·m. Even at the moment of changing load torque, its amplitude is still less than 0.3 N·m. Hence, the proposed controller of torque ripple suppression is not only effective but also has a good dynamic control performance. In order to verify the superiority of the proposed controller, Fig. 13(e) compares the waveform of δT under torque ripple controller and PI controller, turns out that the suppression effect of torque ripple control is more superior than PI control.

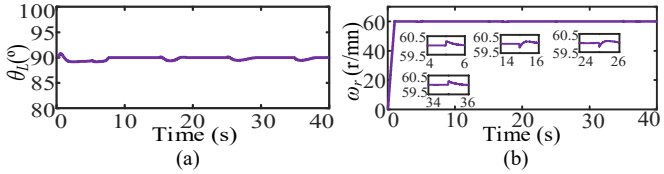

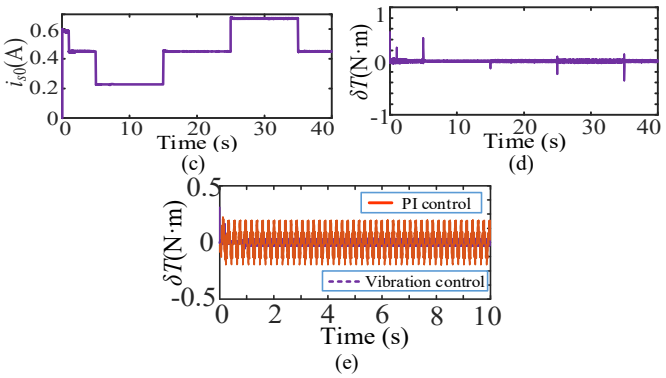

Fig. 13. Waveforms with torque ripple controller in PMSM. (a) θ_L, (b) ω_r, (c) i_{s0}, (d) δT, (e) δT.

The above simulations validate the effectiveness of each independent controller. However, the actual situation is more complex, only a single controller cannot guarantee a good running of PMSM. In the sixth case, various disturbances of flexible load's vibration, harmonic and PMSM's cogging torque and electrical loss are taken into consideration simultaneously. Then, the proposed integrative controller is added. Operating parameters are plotted in Figs. 14(a)-(c), which indicates that the proposed controller ensures a smooth and stable operation of the motor even in various disturbances. Fig. 14(d) gives the waveform of torque ripple δT. Compared to Fig. 11(d), the peak-to-peak value of torque ripple is reduced to less than 0.1 N·m, over 90% of torque ripple has been suppressed effectively. Fig. 14(e) compares the control effect of the proposed integrative controller with and without minimum loss condition on total electrical loss. The result displays that P_{loss} is reduced with the proposed controller effectively.

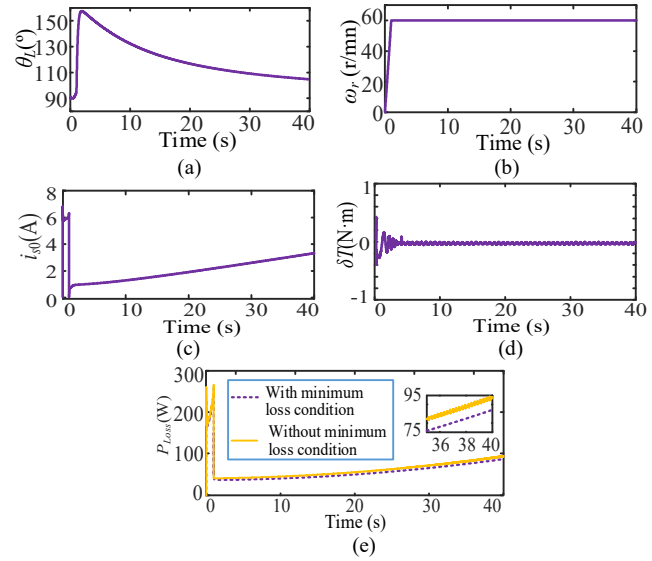

Fig. 14. Waveforms of operating parameters with the proposed closed-loop *I/f* integrative controller. (a) θ_L, (b) ω_r, (c) i_{s0}, (d) δT, (e) P_{Loss}.

C. Hardware Architecture and Experimental Results

The proposed multi-objective backstepping principle-based integrative control scheme is further tested through a hardware platform shown in Fig. 15. The rated power of the PMSM is 550W. DSP TMS320F28335 chip is selected as the control chip. STS is installed in the spring box. STS and PMSM are connected by a spindle, while PMSM drives the spindle to wound STS across a torque sensor. The brake is used to lock the spindle when shutdown. The parameters are consistent with the simulation part.

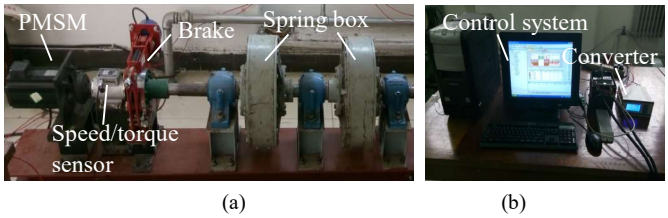

Fig. 15. Hardware platform. (a) PMSM, speed/torque sensor, brake and STS box, (b) control system and inverters.

In the first experiment, PMSM starts up from standstill to 60 r/min by adding the proposed integrative controller, the reference speed increases to 100 r/min at 20 s and recovers to 60 r/min at 30 s. Figs. 16(a)-(c) present the operating variables. Fig. 16(d) gives the waveform of torque ripple δT. Fig. 16(e) compares the results of the integrative controller with and without minimum loss condition, which shows that the proposed integrative controller is able to suppress both vibration and torque, improves the operating efficiency and demonstrates strong robustness to speed switch. In general, the dynamic response of the proposed controller is basically acceptable in changing speed references.

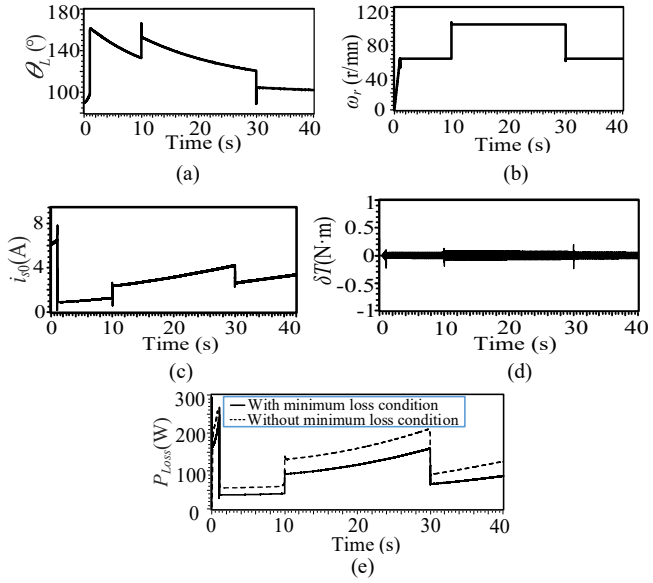

Fig. 16. Operating parameters only with vibration controller and considering electrical loss and torque ripple in PMSM. (a) θ_L, (b) ω_r, (c) i_{s0}, (d) δT, (e) P_{Loss}.

In the second experiment, the minimum loss condition is ignored from 5 s to 10 s, the vibration controller is inactive from 15 s to 20 s, and the torque ripple suppression controller is inactive from 25 s to 30s. At other times, the integrative controller is added. Figs. 17(a)-(c) give the state variables, where the torque ripple δT and total electrical loss P_{Loss} are shown in Figs. 17(d)-(e). The loss of any disturbance controller will affect the control accuracy to some extent. However, the proposed integrative controller enables to improve the control performance of PMSM and ensure energy storage smoother and highly efficient.

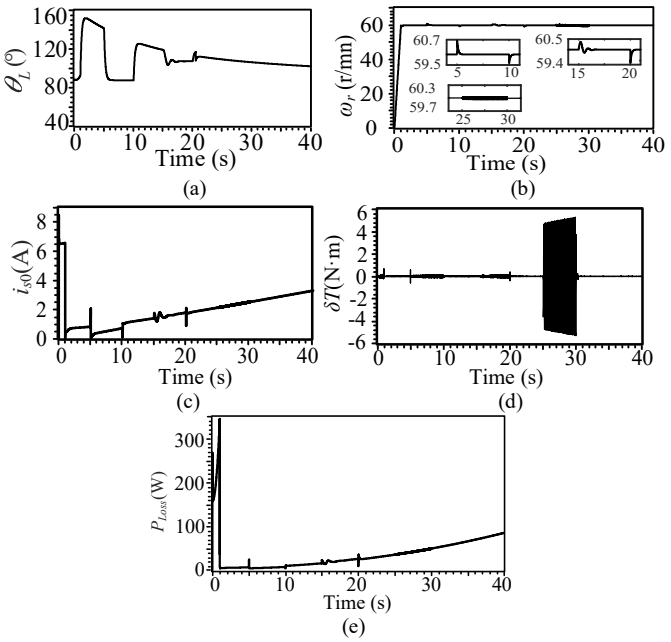

Fig. 17. Operating parameters by adding different control algorithms. (a) θ_L, (b) ω_r, (c) i_{s0}, (d) δT, (e) P_{Loss}.

VI. CONCLUSION

With consideration of the electrical loss of PMSM, a multi-objective nonlinear integrative control scheme is proposed to suppress the vibration of flexible load and torque ripple of PMSM simultaneously. The correctness and effectiveness of the control scenario have been verified through both simulations and experiments. The conclusions are given as follows:

i. Through the proposed integrative control scheme, both the torque ripple of PMSM and the vibration of flexible load are suppressed effectively. Meanwhile, the electrical loss of PMSM is significantly reduced, which improves operating efficiency.

ii. The operating parameters of angle, speed, and current regulated by the integrative control scheme are able to converge to their references rapidly and accurately. Moreover, the parameters' ripple and oscillation hardly happen.

iii. At the moment of a sudden change of reference signal, the overall system is able to keep stability, and only transient and small oscillations have occurred in various state parameters, which indicates that the proposed integrative control has a good dynamic control performance.

iv. The speed identification method on the basis of the least-squares algorithm devised in the research is able to complete the speed identification accurately in a relatively wide region.

REFERENCES

[1] X. G. Tan, Q. M. Li, H. Wang, "Advances and trends of energy storage technology in Microgrid," *Int. J. Elec. Power*, vol. 44, no.1, pp. 179-191, Jan. 2013.

[2] A. B. Gallo, J. R. Simões-Moreir, H. K. M. Costa, M.M. Santos, E. Moutinho dos Santos, "Energy storage in the energy transition context: A technology review," *Renew. Sust. Energ. Rev.*, vol. 65, pp. 800-822, Nov. 2016.

[3] W. Duan and H. C. Feng, "Stress and modal analysis of flat spiral spring in elastic energy storage equipment," *Appl. Mech. Mater.*, vols. 121-126, pp. 1754-1758, Oct. 2012.

[4] J. Q. Tang, Z. Q. Mi, Z. Q. Wang, "Energy storage and stress analysis of spiral spring on mechanical elastic energy storage technology,"in *Proc. Int. Conf. Mech. Electron. Ind. Contr. Eng., Shenyang, China*, *IEEE,* Aug. 2014, pp. 1132-1135.

[5] Y. Yu, Z. Q. Mi, X. D. Guo, X. T. Niu, X. J. Zheng, C. J. Sun, "Control design and implementation of a spiral spring energy storage system connected to a grid via PMSG," *CSEE J. Power. Energ. Syst.*, vol. 4, no. 3, pp. 339-351, 2018.

[6] J. M. Muñoz-Guijosa, D. F. Caballero, V. R. de la Cruz, J. L. M. Sanz, J. Echávarri, "Generalized spiral torsion spring model," *Mech. Mach. Theory*, vol. 51, pp. 110-130, May 2012.

[7] Y. Yu, Z. Q. Mi, X. D. Guo, Y. K. Xu, T. Zhao, "Low speed control and implementation of permanent magnet synchronous motor for mechanical elastic energy storage device with simultaneous variations of inertia and torque," *IET Electr. Power. Appl.*, vol. 10, no. 3, pp. 172-180, Mar. 2016.

[8] T.M. Jahns and Soong W.L., "Pulsating torque minimization techniques for permanent magnet AC motor drives - A review," *IEEE Trans. Ind. Elect.*, vol. 43, no. 2, pp. 321-330, Apr. 1996.

[9] W. Duan, H. C. Feng, M. J. Liu, Z. Q. Wang, "Dynamic analysis and simulation of flat spiral spring in elastic energy storage device," *Asia-Pacific Power Energ. Eng. Conf., Shanghai, China*, pp. 1-4, Sep. 2012.

[10] C. Bianchini, M. Davoli, F. Immovilli, E. Lorenzani, "Design optimization for torque ripple minimization and poles cost reduction with hybrid permanent magnets," in *Proc. 40th Annual Conf. IEEE Ind. Electron. Society*, *Dallas, TX, USA IEEE*, pp. 1553-572X, Feb. 2015.

[11] H. Dhulipati, S. Mukundan, K. L. V. Iyer, N, C. Kar, "Skewing of stator windings for reduction of spatial harmonics in concentrated wound PMSM," in *Proc. 30th Canadian Conference on Electrical and Computer Engineering , Windsor, ON, Canada, IEEE,* June. 2017.

[12] G. D, Feng, C. Y, Lai, N. C. Kar, "Practical Testing Solutions to Optimal Stator Harmonic Current Design for PMSM Torque Ripple Minimization Using Speed Harmonics," *IEEE Trans. Power Electr.*, vol. 33, no.6, pp. 5181-5191, June. 2018.

[13] Y. Yan, W. S. Li, W. T. Deng, G. Z. Zhang, C. L. Xia, "Torque ripple minimization of PMSM using PI type iterative learning control," in *Proc. 40th Annual Conf. IEEE Ind. Electron. Society, Dallas, TX, USA*, *IEEE,* pp. 925-931, Oct. 2015.

[14] Z. Y Zeng, C. Zhu, X. L. Jin, R. X. Zhao, "Hybrid Space Vector Modulation Strategy for Torque Ripple Minimization in Three-Phase Four-Switch Inverter-Fed PMSM Drives," *IEEE Trans. Ind. Electron.*, vol. 64, no. 3, pp. 2122-2134, Mar. 2017.

[15] D. H. Lee, C. L. Jeong, J. Hur, "Analysis of cogging torque and torque ripple according to unevenly magnetized permanent magnets pattern in PMSM," in *Proc. 2017 IEEE Energy Conversion Congress and Exposition*, *Cincinnati, OH, USA*, Nov. 2017.

[16] C. Zhu, Z. Y Zeng, R. X. Zhao, "Torque ripple elimination based on inverter voltage drop compensation for a three-phase four-switch inverter-fed PMSM drive under low speeds," *IET Power Electron.*, vol. 10, no. 12, pp. 1430-1437, Oct. 2017.

[17] H. Ge, Y. Miao, B. Bilgin, B. N. Mobarakeh, A. Emadi, "Speed Range Extended Maximum Torque Per Ampere Control for PM Drives Considering Inverter and Motor Nonlinearities," *IEEE Trans. Power Electr.,* vol. 32, no. 9, pp. 7151-7159, Sept. 2017.

[18] S. Ekanayake, R. Dutta, M. F. Rahman, D. Xiao "Direct torque and flux control of interior permanent magnet synchronous machine in deep flux-weakening region," *IET Electr Power Appl.*, vol. 12, no. 1, pp. 98-105, Jan. 2018.

[19] M. T. Cao and Y. Hori, "Convergence improvement of efficiency-optimization control of induction motor drives," *IEEE Trans. Ind. Appl.*, vol. 37, no. 6, pp. 1746-1753, Nov. 2001.

[20] E. Sergaki, P. Georgilakis, A. Kladas, G. S. Stavrakakis, "Fuzzy logic based online electromagnetic loss minimization of permanent magnet synchronous motor drives," *Int. Conf. Electr. Mach., Vilamoura, Portugal, IEEE,* pp. 6-9, Sep. 2008.

[21] H. Ge, B. Bilgin, A. Emadi, "Global loss minimization control of PMSM considering cross-coupling and saturation," *IEEE Energy Conversion Congress and Exposition.*, *Montreal, Canada*, *IEEE,* pp. 6139-6144, Sep.

2015.

[22] P. H. Truong, F. Damien, N. K. Nguyen, M. Jean, D. M. Tuan, "Optimal Efficiency Control of Synchronous Reluctance Motors-based ANN Considering Cross Magnetic Saturation and Iron Loss," in *Proc. 41st Annual Conf. IEEE Ind. Electron. Society*, *Yokohama, Japan, IEEE,* pp. 4690-4695, Nov. 2015.

[23] Z. Wang, K. Lu, F. Blaabjerg, "A simple startup strategy based on current regulation for back-emf-based sensorless control of PMSM," *IEEE Trans. Power Electr.*, vol. 27, no. 8, pp.3817-3825, Aug. 2012.

[24] G. M. L Gladwell, A. H. England, D. Wang, "Examples of reconstruction of an Euler-Bernoulli beam from spectral data," *J Sound Vib.*, vol. 119, no. 1, pp. 81-94, Nov. 1987.

[25] C. F. Baicu, C. D. Rahn, D. M. Dawson, "Backstepping Boundary Control of Flexible-Link Electrically Driven Gantry Robots," *IEEE-ASME Trans Mech.*, vol. 3, no. 1, pp. 60-66, Mar. 1998.

[26] M. Fatu, R. Teodorescu, I. Boldea, G. D. Andreescu, F. Blaabjerg, "I-F starting method with smooth transition to EMF based motion-sensorless vector control of PM synchronous motor/generator," *IEEE Annual Power Electron. Specialists Conf., Rhodes, Greece*, pp. 1481-1487, June 2008.

[27] Y. S. Ding, X. Xiao, "Research on control strategies of flexible load driven by PMSM,," *Int. Conf. Transportation Electrification Asia-pacific, Beijing, China, IEEE*, pp. 1-5, Aug. 2014.

[28] C. Y. Lai, G. D. Feng, K. Mukherjee, V. Loukanov, N. C. Kar, "Torque ripple modeling and minimization for interior PMSM considering magnetic saturation," *IEEE Trans. Power Electr.*, vol. 33, no. 3, pp. 2417-2429, Mar. 2017.

[29] P. Chapman, S. Sudhoff, C. Whitcomb, "Optimal current control strategies for surface-mounted permanent-magnet synchronous machine drives," *IEEE Trans. Energy. Conver.*, vol. 14, no. 4, pp. 1043-1050, Dec. 1999.

[30] J. H. Jang, S. K. Sul, J. I. Ha, K. Ide, M. Sawamura, "Sensor-less drive of surface mounted permanent magnet motor by high frequency signal injection based on magnetic saliency," *IEEE Trans. Ind. Appl.*, vol. 39, no.4, pp. 1031-1039, July-Aug. 2003.

[31] J. H. Jang, J. I. Ha, M. Ohto, K. Ide, S. K. Sul, "Analysis of permanent-magnet machine for sensor-less control based on high-frequency signal injection," *IEEE Trans. Ind. Appl.*, vol. 40, no.6, pp. 1595-1604, Nov.-Dec. 2004.

[32] C. French and P. Acarnley, "Control of permanent magnet motor drives using a new position estimation technique," *IEEE Trans. Ind. Appl.*, vol. 32, no.5, pp. 1089-1097, Sep./Oct. 1996.

[33] T. Senjyu, T. Shimabukuro, K. Uezato, "Position control of permanent magnet synchronous motors without position and speed sensors," *IEEE PESC Record*, pp 759-765, May 1995.

[34] S. Bolognani, L. Tubiana, M. Zigliotto, "Extended Kalman filter tuning in sensor-less PMSM drives," *IEEE Trans. Ind. Appl.*, vol. 39, no. 6, pp. 1741-1747, Nov. 2003.

[35] S. Bolognani, R. Oboe, M. Zigliotto, "Sensor-less full-digital PMSM drive with EKF estimation of speed and rotor position," *IEEE Trans. Ind. Electron.*, vol. 46, no. 1, pp. 184-191, Feb. 1999.

[36] J. N. Yang, S. Lin, "Identification of parametric variations of structures based on least squares estimation and adaptive tracking technique," *J Eng. Mech.*, vol. 131, no. 3, pp. 290-298, Mar. 2005.

[37] N. Urasaki, T. Senjyu, K. Uezato, "A novel calculation method for iron loss resistance suitable in modeling permanent-magnet synchronous motors," *IEEE Trans. Energy Conver.*, vol. 18, no. 1, pp. 41-47, Mar. 2003.

Yang YU (M'19–) born in Chongqing, China and received the PH.D degree from North China Electric Power University in 2016, Beijing, China. He is an Associate Professor in North China Electric Power University. He have been working as a Visiting Scholar in Lehigh University from 2019 to 2020, Bethlehem, U.S. His main research fields are mechanical elastic energy storage technology and new energy electric power system and intelligent Grid.

Leyao CONG received the B.S. degree from China Three Gorges University in 2017. Currently she is a graduate student in North China Electric Power University. Her main searching fields are mechanical elastic energy storage technology and new energy electric power system and intelligent Grid.

Xia TIAN received the B.S. degree from North China Electric Power University in 2017. Currently she is a graduate student in North China Electric Power University. His main searching fields are mechanical elastic energy storage technology and new energy electric power system and intelligent Grid.

Zengqiang MI born in 1960, currently he is a professor and doctoral tutor in North China Electric Power University. His main fields are mechanical elastic energy storage technology and new energy electric power system and intelligent Grid etc.

Yang LI (S'13–M'14–SM'18) born in Nanyang, China. He received his Ph.D. degree in Electrical Engineering from North China Electric Power University (NCEPU), Beijing, China, in 2014. He is an Associate professor at the School of Electrical Engineering, Northeast Electric Power University, Jilin, China. From Jan. 2017 to Feb. 2019, he was also a postdoc with Argonne National Laboratory, Lemont, U.S. His research interests include power system stability and control, renewable energy integration, energy storage and smart grids. He serves as an Associate Editor for the journals of IEEE ACCESS and Electrical Engineering.

Zhen FAN received the B.S. degree and M.S. degree from North China Electric Power University in 2017 Baoding, C.N. and Lehigh University in 2020, Bethlehem, U.S.. Currently, he is pursuing the doctor degree in Lehigh University, Bethlehem, U.S. His main research fields are power electronics and microgrids.